

Determination of local structure in solid nucleic acids using double quantum nuclear magnetic resonance spectroscopy

D. M. Gregory

Department of Physics, University of Washington, Seattle, Washington 98195

M. A. Mehta and J. C. Shiels

Department of Chemistry, University of Washington, Seattle, Washington 98195

G. P. Drobny

Departments of Chemistry and Physics, University of Washington, Seattle, Washington 98195

(Received 26 July 1996; accepted 12 March 1997)

A theoretical analysis of dipolar recoupling with a windowless multipulse irradiation (DRAWS) is presented. Analytical expressions that describe the degree to which the DRAWS pulse sequence recouples the dipolar interaction as a function of offset and spinning rate are derived using Floquet theory. Numerical methods are used to assess the performance of DRAWS in the preparation and detection of multiple quantum coherence. Simulations indicate that the mutual orientation of two or more CSA tensors can be obtained with high accuracy from double quantum spectra prepared and detected by DRAWS irradiation (DQDRAWS). These expectations are born out by experiment and in particular, the mutual orientation of three ^{13}C CSA tensors in selectively labeled 2'-deoxythymidine are determined from DQDRAWS data. The results of the DQDRAWS analysis of CSA tensor orientation in 2'-deoxythymidine are shown to be in excellent agreement with results obtained by conventional methods. Using these CSA tensor orientations and an independent measurement of internuclear distance, a practical strategy is proposed and executed for deriving the mutual orientation of purine and pyrimidine bases in a DNA dodecamer from DQDRAWS data. The DQDRAWS method for determining the mutual orientation of rigid bodies in macromolecules is compared and contrasted to distance-based methods. © 1997 American Institute of Physics. [S0021-9606(97)02023-0]

I. INTRODUCTION

Multiple quantum NMR transitions are coherent superpositions of Zeeman states that violate the dipolar selection rule: $|\Delta m| = 1$. Observed over forty years ago in the saturated, continuous wave, high-resolution NMR spectra of liquids,¹⁻³ multiple quantum transitions are now most commonly prepared and detected by multidimensional methods.⁴ In high-resolution NMR, multiple quantum pulse sequences are familiar components of experiments intended to elucidate the solution structure of biological macromolecules.⁵

Multiple quantum spectroscopy has recently been incorporated into magic angle spinning (MAS) experiments where the preparation of multiple quantum coherence is complicated by the fact that high speed spinning at the "magic angle," which removes the anisotropic chemical shift and heteronuclear dipolar couplings, removes to lowest order the homonuclear dipolar interactions as well.⁶⁻⁸ Under MAS conditions multiple quantum coherence may be prepared by placing the coupled spins in rotational resonance.⁹⁻¹⁴ Alternatively, multipulse dipolar recoupling techniques have been used to prepare double quantum coherence with varying degrees of success. For example, Meier and Earl applied a multiple quantum "time reversal" pulse sequence during MAS to prepare proton multiple quantum coherence in adamantane.¹⁵

In many cases, double quantum coherence has been used as a spectral filter, where only single quantum transitions arising from coupled spins are detected once coherence is

transferred through a double quantum stage.¹⁶ Such studies have demonstrated that double quantum coherence can be very efficiently prepared during MAS under certain circumstances. For example, using first order rotational resonance, Nielsen *et al.*¹⁷ demonstrated preparation of double quantum coherence with 50% efficiency in doubly ^{13}C -labeled zinc acetate. Tycko and co-workers used DRAMA¹⁸ and a DRAMA¹⁹ supersequence to achieve double quantum filtered ^{13}C spectra in a number of oligopeptides. Other novel dipolar recoupling pulse sequences including C7²⁰ and DRAWS²¹ have been used to produce double quantum filtered spectra.

Structural information may be obtained from an analysis of the sidebands intensities of a multiple quantum MAS spectrum. The intensities of the fundamental peak of the double quantum spectrum of two coupled spin-1/2 nuclei and the attendant side bands, contain information on the internuclear distance, as shown by the proton double quantum experiments of Spiess and co-workers.^{22,23} In addition, information on the mutual orientation of the chemical shift tensors and the orientation of the internuclear vector relative to the principal axis systems of the CSA tensors of the two spins can be obtained even in situations where neither single crystals nor aligned samples of any kind are available. Furthermore, unlike rotational resonance which is spectrally selective, multiple quantum techniques can determine CSA tensor orientations over a broad spectral range.

The purpose of this paper is to provide a theoretical de-

DQ-DRAWS Sequence

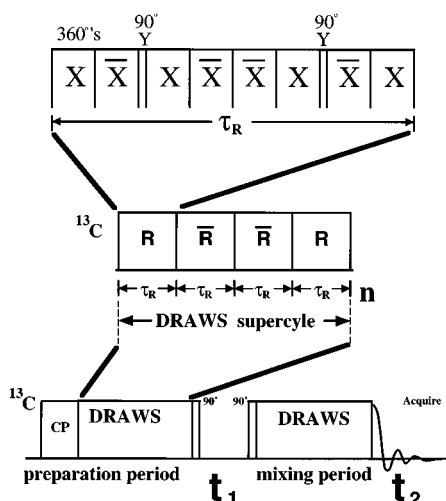


FIG. 1. Double quantum MAS pulse sequences using DRAWS in the preparation and the mixing periods (DQDRAWS). Preparation of double quantum coherence is performed with an initial state $\rho(0) = I_x + S_x$.

scription of the preparation and detection of multiple quantum coherence in systems of dipolar coupled spin-1/2 nuclei in rotating solids using a windowless dipolar recoupling pulse sequence (DRAWS).²⁴ Numerical calculations of and analytical expressions for the intensities of the fundamental and the sideband transitions of the double quantum spectrum of two coupled spin-1/2 nuclei will be presented and the degree to which such spectra provide detailed structural information in nucleic acids will be considered. By way of example, the orientation of three ¹³C CSA tensors in 2'-deoxythymidine will be determined from double quantum DRAWS (DQDRAWS) data. It is then shown how these tensor orientations, together with an independent measurement of internuclear distance, can be used to determine the mutual orientation of pyrimidine base planes in an isotopically-labeled DNA dodecamer using DQDRAWS.

II. THEORY

Here we derive using Floquet theory^{25–29} and second order perturbation theory, the theoretical basis for dipolar recoupling with the DRAWS pulse sequence. The degree to which DRAWS is useful for preparing and detecting double quantum coherence will then be described using numerical methods.

A. The DRAWS Floquet Hamiltonian

We are interested in calculating the degree to which the dipolar Hamiltonian is recoupled as a result of irradiating an ensemble of dipolar-coupled spin-1/2 pairs with the DRAWS pulse sequence shown in Fig. 1. The calculation begins with the definition of the spin interaction MAS Hamiltonian $H(t)$

$$H(t) = H_{\text{rf}}(t) + H_{\text{int}}(t), \quad (1a)$$

where

$$H_{\text{rf}}(t) = \omega_{\text{rf}} [2I_x^{1-2} \cos \varphi(t) - 2I_y^{2-3} \sin \varphi(t)] \quad (1b)$$

and

$$H_{\text{int}}(t) = -\omega_{\Sigma}(t) I_x^{1-3} - \omega_{\Delta}(t) I_x^{2-4} + \omega_D(t) \left[\frac{3}{2} I_z^{1-2} - \frac{1}{2} (I_z^{1-3} + I_z^{2-3}) \right]. \quad (1c)$$

The fictitious spin-1/2 angular momentum operators^{37,38} I_k^{i-j} are defined using a “strong coupling” basis set:

$$\begin{aligned} |1\rangle &= \frac{i}{\sqrt{2}} (|\alpha\alpha\rangle + |\beta\beta\rangle), & |2\rangle &= \frac{i}{\sqrt{2}} (|\alpha\beta\rangle + |\beta\alpha\rangle), \\ |3\rangle &= -\frac{i}{\sqrt{2}} (|\alpha\alpha\rangle - |\beta\beta\rangle), & |4\rangle &= -\frac{i}{\sqrt{2}} (|\alpha\beta\rangle - |\beta\alpha\rangle). \end{aligned} \quad (2)$$

In Eq. (1) the definitions $\omega_{\Sigma}(t) = \omega_I(t) + \omega_S(t)$ and $\omega_{\Delta}(t) = \omega_I(t) - \omega_S(t)$ have been used. The time-dependent chemical shifts for spins I and S , $\omega_I(t)$ and $\omega_S(t)$, and the time-dependent dipolar interaction $\omega_D(t)$ are expressed as Fourier expansions in ω_R , the spinning rate:

$$\omega_{I,S}(t) = \frac{\omega_0}{2\pi} \left(\sigma_{I,S} + \sqrt{\frac{3}{2}} \sum_{n=-2}^{+2} \omega_n^{I,S} e^{-in\omega_R t} \right)$$

and

$$\omega_D(t) = \sum_{n=-2}^{+2} \omega_n^D e^{-in\omega_R t}, \quad (3a)$$

where

$$\begin{aligned} \omega_{\pm n}^{I,S} &= d_{\pm n,0}^{(2)}(\theta) e^{\mp in\gamma} \sum_{m=-2}^{+2} [A_{2,2}^{I,S} \{D_{-2,m}^{(2)}(\Omega_{I,S}) + D_{2,m}^{(2)}(\Omega_{I,S})\} \\ &\quad + A_{2,0}^{I,S} D_{0,m}^{(2)}(\Omega_{I,S})] e^{-iam} d_{-2,\pm n}^{(2)}(\beta) \end{aligned} \quad (3b)$$

and

$$\begin{aligned} \omega_{\pm n}^D &= \frac{\mu_0}{4\pi} \frac{\gamma_I \gamma_S \hbar}{r^3} d_{\pm n,0}^{(2)}(\theta) e^{\mp in\gamma} \\ &\quad \times \sum_{q=-2}^{+2} D_{0,q}^{(2)}(\Omega_D) d_{q,\pm n}^{(2)}(\beta) e^{-iq\alpha}. \end{aligned} \quad (3c)$$

In Eqs. (3a)–(3c) all symbols have their usual definitions. The dipolar coupling constant is defined as

$$\omega_{IS} = \frac{\mu_0}{4\pi} \frac{\hbar \gamma_I \gamma_S}{r^3},$$

where γ_I and γ_S are the magnetogyric ratios of spins I and S , respectively, and μ_0 is the free space permeability. The anisotropy of the chemical shift tensor is $A_{2,0}^{I,S} = \sqrt{\frac{3}{2}} (\sigma_{33}^{I,S} - \sigma_{I,S})$ and the asymmetry of the chemical shift tensor is $A_{2,2}^{I,S} = \frac{1}{2} (\sigma_{11}^{I,S} - \sigma_{22}^{I,S})$. The Euler angles $\Omega_{I,S} = (\alpha_{I,S}, \beta_{I,S}, \gamma_{I,S})$ relate the principal axis frames of the CSA tensors of spins I and S to a crystal-fixed axis frame, and the Euler angles $\Omega_D = (0, \beta_D, \gamma_D)$ similarly relate the principal axis frame of the dipolar tensor to a crystal-fixed axis frame. Finally, the angles (α, β, γ) relate the crystal-fixed

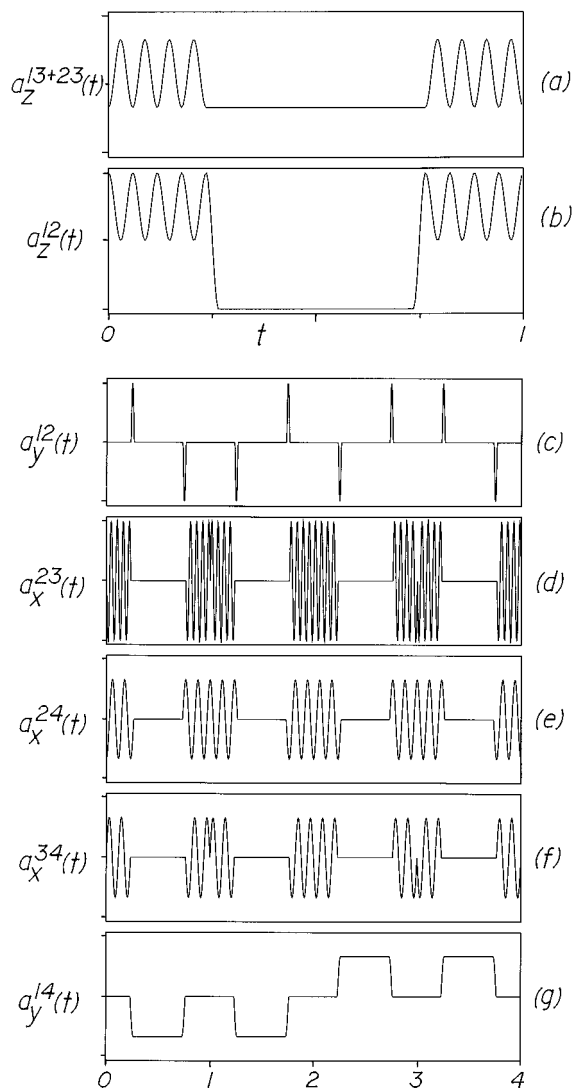


FIG. 2. Time-dependent coefficients for the operators in the interaction frame Hamiltonian corresponding to irradiation of two dipolar coupled spins by the DRAWS pulse sequence in (a). In all frames the horizontal axis is time in units of τ_c , the DRAWS pulse cycle. The dipolar operators $I_z^{1-3} + I_z^{2-3}$ and I_z^{1-2} have coefficients that have period τ_c . Other operators have period $4\tau_c$.

frame to the goniometer frame, and $(\omega_R t, \theta, 0)$ relate the goniometer frame to the laboratory frame. In an MAS experiment it is assumed that $\theta = \cos^{-1}(1/\sqrt{3})$.

The DRAWS Hamiltonian is calculated in an interaction frame defined by the transformation $U_{\text{rf}}(t) = e^{-iH_{\text{rf}}(t)}$. In practice, the DRAWS pulse sequence shown in Fig. 1 is used, but in the calculation that follows, a slightly simplified DRAWS sequence is assumed in which the phase-alternated 360° pulses are replaced by continuous single phase irradiation. Under these conditions, the interaction frame Hamiltonian $\tilde{H}(t)$ has the form

$$\begin{aligned} \tilde{H}(t) = & \omega_D(t) [a_z^{12}(t) I_z^{1-2} + a_z^{13+23}(t) (I_z^{1-3} + I_z^{2-3}) \\ & + a_x^{23}(t) I_x^{2-3} + a_y^{12}(t) I_y^{1-2}] \\ & + \omega_\Delta(t) [a_x^{24}(t) I_x^{2-4} + a_x^{34}(t) I_x^{3-4} + a_y^{14}(t) I_y^{1-4}]. \quad (4) \end{aligned}$$

In Eq. (4) it is assumed that the rf has been selected such that the offset of spin 1's isotropic peak from resonance $\Delta\omega_1 = -\Delta\omega_2$, the offset of the isotropic peak of spin 2. This assumption results in $\omega_\Sigma(t) = 0$. The coefficients $a_p^{ij}(t)$ for the dipolar terms in the DRAWS interaction frame Hamiltonian are shown in Fig. 2. Under DRAWS irradiation the dipolar coefficients a_z^{12} , a_z^{13+23} have a period equal to $\tau_R = (2\pi)/\omega_R$, the period of the spinning. On the other hand the dipolar coefficients a_x^{23} , a_y^{12} , and the chemical shift coefficients a_x^{24} , a_x^{34} , and a_y^{14} have a period $4\tau_R$.

A time-independent form for the DRAWS Hamiltonian may be obtained using Floquet theory. Floquet's theorem^{25,26} asserts that for a periodic Hamiltonian $\tilde{H}(t)$ with period τ , the quantum mechanical time displacement operator $U(\tau)$ has the form

$$U(\tau) = P(\tau) e^{-iH_F \tau}, \quad (5)$$

where $P(\tau)$ is periodic with period τ and H_F is a time-independent characteristic constant, the "Floquet Hamiltonian." Given a time-dependent Hamiltonian $\tilde{H}(t)$ with period $\tau = (2\pi)/\omega$ the matrix elements of the Floquet Hamiltonian H_F are defined as²⁷

$$\begin{aligned} \langle pn | H_F | qm \rangle = & \frac{1}{\tau} \int_0^{\tau=2\pi/\omega} dt \langle p | \tilde{H}(t) | q \rangle e^{-i(n-m)\omega t} \\ & + n\omega \delta_{nm} \delta_{pq}. \quad (6) \end{aligned}$$

Therefore, in order to obtain an expression for the DRAWS Floquet Hamiltonian, the time-dependent coefficients $a_p^{ij}(t)$ in Eq. (4) must be expressed as Fourier expansions in $\omega_R/4$. For DRAWS these Fourier expansions converge rapidly and in general less than 200 Fourier coefficients are required to accurately calculate the functions $a_p^{ij}(t)$.

Given the interaction frame Hamiltonian in Eq. (4), using Eq. (6) and the Fourier expansion coefficients for $\omega_D(t)$, $\omega_\Delta(t)$, and the $a_p^{ij}(t)$'s, the DRAWS Floquet Hamiltonian has the form

$$\begin{aligned} H_F = & \frac{\omega_R}{4} \sum_{k=1}^4 N^{kk} + \sum_{n=-\infty}^{+\infty} \sum_{m=-2}^{+2} \omega_{4m}^D [a_{z,n-4m}^{12} Z_n^{12} \\ & + a_{z,n-4m}^{13+23} (Z_n^{13} + Z_n^{23}) + a_{x,n-4m}^{23} X_n^{23} + a_{y,n-4m}^{12} Y_n^{12}] \\ & + \sum_{n=-\infty}^{+\infty} \sum_{m=-2}^{+2} \omega_{4m}^\Delta [a_{x,n-4m}^{24} X_n^{24} + a_{x,n-4m}^{34} X_n^{34} \\ & + a_{y,n-4m}^{14} Y_n^{14}], \quad (7) \end{aligned}$$

where the pseudo-spin-1/2 Floquet operators introduced by Schmidt and Vega³⁰ have been used. The index shift in the Fourier coefficients of the dipolar coupling constant and the chemical shielding is necessitated by the supercycle which has a period of $4\tau_R$, as mentioned above and in Weintraub and Vega.²⁹

Note the more complicated form of the DRAWS Floquet Hamiltonian in comparison to the DRAMA Floquet Hamiltonian, which was calculated in Ref. 29 using a "delta pulse" approximation. The dipolar Floquet operator X_n^{23} and the more complicated time dependence of $Z_n^{13} + Z_n^{23}$ in the

DRAWS Floquet Hamiltonian results from the continuous y irradiation, while the operator Y_n^{12} is a result of the finite nature of the x pulses of the DRAWS sequence. Finite pulse effects also result in three chemical shift operators in the DRAWS Floquet Hamiltonian: X_n^{24} , X_n^{34} , Y_n^{14} .

B. Effective DRAWS Hamiltonian: Perturbation theory

Perturbative methods may be used to obtain approximate eigenvalues for the DRAWS Floquet Hamiltonian^{30–35} or

$$\begin{aligned}
 H_F \approx & \frac{\omega_R}{4} \sum_{k=1}^4 N^{kk} + Z_0^{12} \left\{ z_0^{12} - z_0^{13+23} - \left(\frac{4}{\omega_R} \right)^2 \sum_{k=1}^{\infty} \frac{1}{k^2} \left[z_0^{12} |y_k^{12}|^2 + (z_0^{12} - 3z_0^{13+23}) |x_k^{23}|^2 - \frac{(z_0^{12} - z_0^{13+23})}{2} |x_k^{24}|^2 \right] \right\} \\
 & + Z_0^{13} \left\{ 2z_0^{13+23} - \left(\frac{4}{\omega_R} \right)^2 \sum_{k=1}^{\infty} \frac{1}{k^2} [z_0^{13+23} |x_k^{34}|^2 - (z_0^{12} - 3z_0^{13+23}) |x_k^{23}|^2] \right\} \\
 & + Z_0^{14} \left(\left(\frac{4}{\omega_R} \right)^2 \sum_{k=1}^{\infty} \left\{ \frac{1}{k^2} [z_0^{13+23} |x_k^{34}|^2 + \left(\frac{z_0^{12} - z_0^{13+23}}{2} \right) |x_k^{24}|^2 + \left(\frac{z_0^{12} + z_0^{13+23}}{2} \right) |y_k^{14}|^2] \right\} \right), \quad (8)
 \end{aligned}$$

where $z_0^{12}/2 = a_{z,8}^{12} \text{Re}(\omega_8^D) + a_{z,4}^{12} \text{Re}(\omega_4^D)$, $z_0^{13+23}/2 = a_{z,8}^{13+23} \text{Re}(\omega_8^D) + a_{z,4}^{13+23} \text{Re}(\omega_4^D)$, and x_k^{23} , x_k^{24} , x_k^{34} , y_k^{12} , y_k^{14} are products of Fourier coefficients as described in Ref. 29.

Evaluating the series:

$$\sum_{k=1}^{\infty} \frac{|y_k^{12}|^2}{k^2}, \sum_{k=1}^{\infty} \frac{|x_k^{23}|^2}{k^2}, \sum_{k=1}^{\infty} \frac{|y_k^{14}|^2}{k^2}, \sum_{k=1}^{\infty} \frac{|x_k^{24}|^2}{k^2}, \sum_{k=1}^{\infty} \frac{|x_k^{34}|^2}{k^2},$$

and expressing z_0^{12} and z_0^{13+23} in terms of ω_8^D and ω_4^D , we obtain in the limit $\omega_R > \Delta\omega > \omega_D$ the effective Hamiltonian for DRAWS:

$$\begin{aligned}
 \bar{H}_{\text{eff}}^D \approx & [\text{Re}(\omega_4^D) - \frac{1}{10} \text{Re}(\omega_8^D)] \left[1 - 0.002 \left(\frac{\Delta\omega}{\omega_R} \right)^2 \right] \hat{I}_Z^{1-2} \\
 & + [\text{Re}(\omega_4^D) + \frac{1}{10} \text{Re}(\omega_8^D)] \left[1 - 0.010 \left(\frac{\Delta\omega}{\omega_R} \right)^2 \right] \hat{I}_Z^{1-3} \\
 & - 2 \text{Re}(\omega_4^D) \left(\frac{\Delta\omega}{\omega_R} \right)^2 \hat{I}_Z^{1-4}. \quad (9)
 \end{aligned}$$

The recoupled dipolar interaction \bar{H}_{eff}^D is represented by the first two terms in Eq. (9). The scaling of the recoupled dipolar interaction is the ratio of the magnitude of the recoupled dipolar interaction to the magnitude of the static dipolar interaction. In general the recoupling is dependent upon orientation so to estimate the dipolar scaling it is useful to calculate the orientationally averaged matrix norm of the recoupled dipolar Hamiltonian $\|\bar{H}_{\text{eff}}^D\|$ which has the form

eigenvalues can be obtained by numerical diagonalization. We will use a perturbative approach first in order to obtain some physical intuition about the manner in which DRAWS recouples dipolar interactions and thus the efficiency with which it effects preparation of double quantum coherence. Details are given in the Appendix. It can be shown that the perturbation expansions for the eigenvalues of the Floquet Hamiltonian converge rapidly when $\omega_R > \Delta\omega$, where $\Delta\omega = \Delta\omega_1 - \Delta\omega_2$.²⁹ In this limit to second order the DRAWS Floquet Hamiltonian is

$$\begin{aligned}
 \|\bar{H}_{\text{eff}}^D\|^2 &= \frac{1}{4\pi} \int_0^{2\pi} d\gamma \int_0^\pi d\beta \sin\beta \text{Tr}[(\bar{H}_{\text{eff}}^D)^2] \\
 &\approx \frac{\omega_{IS}^2}{20} \left[1 - 0.012 \left(\frac{\Delta\omega}{\omega_R} \right)^2 + 0.0001 \left(\frac{\Delta\omega}{\omega_R} \right)^4 \right]. \quad (10)
 \end{aligned}$$

The matrix norm given in Eq. (10) can be used to calculate a dipolar scaling parameter for DRAWS:

$$\begin{aligned}
 S_{\text{DRAWS}} &= \frac{\|\bar{H}_{\text{eff}}^D\|}{\|H_{\text{static}}^D\|} = \frac{1}{2\sqrt{2}} \left[1 - 0.012 \left(\frac{\Delta\omega}{\omega_R} \right)^2 \right. \\
 &\quad \left. + 0.0001 \left(\frac{\Delta\omega}{\omega_R} \right)^4 \right]^{1/2}. \quad (11)
 \end{aligned}$$

In the fast spinning limit, Eq. (11) indicates a dipolar scaling of about 0.36, and a weak dependence on offset. Both results have been predicted by numerical calculations and observed experimentally.²⁴

C. Preparation, evolution, and detection of multiple quantum coherence using DRAWS

During the double quantum preparation period, DRAWS irradiation is applied synchronously with the sample spinning, and so the preparation time is equal to an integral number of rotational cycles, i.e., $\tau = N\tau_C = N \times M \times \tau_R = N \times M \times (2\pi)/\omega_R$. Assuming that the initial density operator has the form $\rho(0) = \hat{I}_Z + \hat{S}_Z = 2\hat{I}_X^{1-3}$, the efficiency of double quantum preparation by DRAWS irradiation is given by

$$\begin{aligned} & \text{Tr}[U_F(\tau)I_X^{1-3}U_F^{-1}(\tau)I_Y^{1-3}] \\ &= \sum_{m \neq n} I_{m,n} \sin[(\mu_{m,0} - \mu_{n,0})N\tau_C] \\ &= \sum_{m \neq n} I_{m,n} \sin(\Delta\mu_{mn}N\tau_C), \end{aligned} \quad (12)$$

where $\mu_{m,k}$ is the eigenvalue of the DRAWS Floquet Hamiltonian corresponding to the m th Zeeman state and the k th Floquet state.

Specific structural information is obtained from individual double quantum sideband intensities, which in turn requires an expression for the evolution of double quantum coherence. Double quantum coherence, prepared by DRAWS irradiation, evolves during t_1 under the Hamiltonian

$$\begin{aligned} H(t_1) &= \omega_\Sigma(t_1)I_X^{1-3} \\ &= \omega_0 I_X^{1-3} \left[\sqrt{\frac{3}{2}} \sum_{n=-2}^{+2} (\omega_n^I + \omega_n^S) e^{-in(\omega_R t_1 + \gamma)} \right]. \end{aligned} \quad (13)$$

It is easy to show that the Floquet Hamiltonian relevant to the evolution of double quantum coherence is

$$H_F = \omega_R(N^{11} + N^{33}) + \sum_{n=-2}^{+2} x_n^{1-3} X_n^{13}, \quad (14)$$

where $x_{\pm n}^{1-3} = (\omega_{\pm n}^I + \omega_{\pm n}^S) e^{\mp in\gamma}$. The evolution of double quantum coherence under the Floquet Hamiltonian in Eq. (14) is mathematically equivalent to the evolution of an isolated spin-1/2 nucleus subjected to a shaped irradiation, described by Goelman *et al.*³⁵ As in the shaped irradiation problem, the Floquet Hamiltonian in Eq. (14) can be diagonalized analytically

$$DH_F D^{-1} = \omega_R(N^{11} + N^{33}) + x_0^{1-3} Z_0^{13}, \quad (15)$$

where

$$D = \exp\left(\sum_{n \neq 0} \frac{x_n^{1-3}}{n\omega_R} Z_n^{13}\right) \exp\left(-i\frac{\pi}{2} Y_0^{13}\right).$$

The evolution of multiple quantum coherence is calculated by evaluation of the trace $\text{Tr}[U(t_1)I_Y^{1-3}U^{-1}(t_1)I_Y^{1-3}]$, which proceeds in a manner analogous to the calculation of the MAS spectrum of an isolated spin-1/2 nucleus

$$\begin{aligned} & \text{Tr}[U(t_1)I_Y^{1-3}U^{-1}(t_1)I_Y^{1-3}] \\ &= -\frac{1}{4} \sum_{m,n} d_n^{1-3} (d_m^{1-3})^* \cos[(m-n)\omega_R t_1], \end{aligned} \quad (16)$$

where

$$\begin{aligned} d_m^{1-3} &= \sum_k J_k\left(\frac{-|x_1^{1-3}|}{\omega_R}\right) J_{m-2k}\left(\frac{-|x_2^{1-3}|}{2\omega_R}\right) \\ &\quad \times e^{i(k\varphi_1 + (m-2k)\varphi_2)}, \quad x_n^{1-3} = |x_n^{1-3}| e^{i\varphi_n}, \end{aligned}$$

and

$$J_n(x) = \sum_{k \geq 0} \frac{(-)^k}{k!(k+n)!} \left(\frac{x}{2}\right)^{2k+n}$$

is an integral Bessel function of order n .

Because t_1 is not generally incremented in integral multiples of the rotor period, the Euler angle γ is a function of t_1 i.e., $\gamma(t_1) = \gamma_0 + \omega_R t_1$ and the Fourier components in the expansion of $\omega_D(t)$ during the mixing period become functions of t_1 as well

$$\begin{aligned} \omega_{\pm n}^D(t_1) &= \frac{\mu_0}{4\pi} \frac{\gamma_1 \gamma_S \hbar}{2\pi r^3} d_{\pm n,0}^{(2)}(\theta) e^{\mp in\gamma(t_1)} \\ &\quad \times \sum_{q=-2}^{+2} D_{0,q}^{(2)}(\Omega_D) d_{q,\pm n}^{(2)}(\beta) e^{-iq\alpha}. \end{aligned} \quad (17)$$

When the mixing period is of duration $N\tau_C$ the mixing dynamics can be described by the trace

$$\begin{aligned} & \text{Tr}[U(N\tau_C)I_Y^{1-3}U^{-1}(N\tau_C)I_X^{1-3}] \\ &= \frac{i}{4} (-U_{11}U_{33}^{-1} - U_{13}U_{13}^{-1} + U_{31}U_{31}^{-1} + U_{33}U_{11}^{-1}) \\ &= \sum_{u \neq v} I_{u,v} \sin\{[\mu_{u,0}(t_1) - \mu_{v,0}(t_1)]N\tau_C\}, \end{aligned} \quad (18)$$

which in the limit $\Delta\omega \ll \omega_R$ reduces to

$$\text{Tr}[U(N\tau_C)I_Y^{1-3}U^{-1}(N\tau_C)I_X^{1-3}]$$

$$\propto \sin\left[\frac{3}{2} \text{Re}(\omega_4^D)N\tau_C \cos \omega_R t_1\right]$$

or

$$\text{Tr}[U(N\tau_C)I_Y^{1-3}U^{-1}(N\tau_C)I_X^{1-3}]$$

$$\propto \sum_{k=0}^{\infty} (-)^k J_{2k+1}\left[\frac{3}{2} \text{Re}(\omega_4^D)N\tau_C\right] \cos[(2k+1)\omega_R t_1].$$

(19)

Therefore, DRAWS irradiation during the mixing period recouples the dipolar interaction, but this interaction is now a function of t_1 so long as the length of the evolution period is not an integral multiple of the spinning period.

D. Dependence of the DQDRAWS spectrum on structure: Numerical simulations

Equation (18) means that the recoupled dipolar interaction is introduced directly into the double quantum spinning side band intensities as a result of DRAWS irradiation during the mixing period as opposed to the preparation Hamiltonian which affects only the intensity of the overall spectrum. Therefore, the individual side band intensities in the double quantum DRAWS (DQDRAWS) spectrum, as well as the integrated intensity of the DQDRAWS spectrum are affected by the details of the dipolar recoupling sequence. Even if negligible chemical shift evolution occurs during t_1 , sidebands will be observed in the double quantum spectrum as a result of the dipolar modulation predicted by Eq. (19), although no isotropic peak would be observed and only even

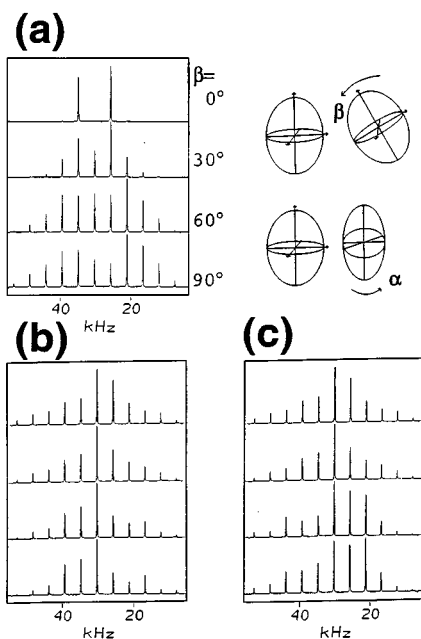


FIG. 3. Calculated DQDRAWS spectra showing the effect of different chemical shift tensor and dipolar tensor orientations. The principal values for the CSA tensors for C4 and C6 in 2'-deoxythymidine-4,6- $^{13}\text{C}_2$ have been used (see Table I) and $\nu_R = 4525$ Hz. (a) In the top spectrum the PAS frames for C4 and C6 are coincident so the double quantum tensor elements are $\sigma_{11}^{\text{DQ}} = \sigma_{11}^{\text{C4}} + \sigma_{11}^{\text{C6}} = 286$ ppm, $\sigma_{22}^{\text{DQ}} = \sigma_{22}^{\text{C4}} + \sigma_{22}^{\text{C6}} = 289$ ppm, and $\sigma_{33}^{\text{DQ}} = \sigma_{33}^{\text{C4}} + \sigma_{33}^{\text{C6}} = 329$ ppm. In the spectra below the β angle of the C4 carbon has been incremented in 30° steps. In the bottom spectrum the double quantum tensor elements are $\sigma_{11}^{\text{DQ}} = \sigma_{33}^{\text{C4}} + \sigma_{11}^{\text{C6}} = 135$ ppm, $\sigma_{22}^{\text{DQ}} = \sigma_{22}^{\text{C4}} + \sigma_{22}^{\text{C6}} = 298$ ppm, and $\sigma_{33}^{\text{DQ}} = \sigma_{11}^{\text{C4}} + \sigma_{33}^{\text{C6}} = 480$ ppm. The larger anisotropy results in a greater number of sidebands in the DQDRAWS spectrum. (b) In the top spectrum Euler angles appropriate for 2'-deoxythymidine-4,6- $^{13}\text{C}_2$ have been used (see Fig. 7). These are, for C4, $\alpha = 84^\circ$, $\beta = 90^\circ$, and $\gamma = 180^\circ$ and for C6, $\alpha = 90^\circ$, $\beta = 54^\circ$, and $\gamma = 90^\circ$. In the spectra below the β angle of the C4 carbon has been incremented in 30° steps. (c) Same as (b) but the Euler angle α is incremented in 30° steps.

order side bands would have nonzero intensity. This effect has been reported and exploited by Spiess and co-workers³⁸ who have observed at high spinning rates side-banded double quantum spectra for systems of coupled proton pairs. In addition to being sensitive to the principal values of the two chemical shift tensors and the internuclear distance, all of which can be measured by independent methods, DQDRAWS side band intensities are sensitive to five Euler angles: The three components of the solid Euler angle relating the principal axis frames of the two chemical shift tensors, and the two angles orienting the internuclear vector in a reference frame common to the two chemical shift tensors.

As an example of the degree to which DQDRAWS data elucidates local structure, consider two dipolar-coupled ^{13}C spins with shift tensors (in units of ppm): C1($\sigma_{11}, \sigma_{22}, \sigma_{33}$) = (242, 168, 91) and C2($\sigma_{11}, \sigma_{22}, \sigma_{33}$) = (44, 130, 238). Assume the two spins are separated by 2.5 Å. Figure 3 illustrates the effect on the double quantum spectrum of varying the mutual orientation of the CSA tensors of the two ^{13}C spins. In Fig. 3(a), the two CSA tensors begin in a collateral arrangement for which $(\alpha, \beta, \gamma) = (0, 0, 0)$, represented by the spectrum in the top lane, and β is incremented by 30° in the

lower lanes. The trend in Fig. 3(a) can be easily explained if we realize that for $\beta = 0$, the effective double quantum chemical shift tensor has elements $(\sigma_{11}^{\text{DQ}}, \sigma_{22}^{\text{DQ}}, \sigma_{33}^{\text{DQ}}) = (286, 289, 329)$, and so the top trace corresponds to a double quantum spectrum dominated by the anisotropy of the dipolar interaction [see Eq. (19)]. As β is incremented from 0° the influence of the chemical shift anisotropy becomes more pronounced in the double quantum spectrum as the even order side bands and fundamental peak gradually increase in intensity. Figures 3(b) and 3(c) show the same effect for a different initial orientation of the shift tensors.

Equations (16) and (19), and the simulations in Fig. 3 suggest a method for determining the mutual orientation of rigid bodies within macromolecules from DQDRAWS data. For the purposes of this discussion, a rigid structure is defined as a network of covalently bonded atoms that are constrained on average, to lie at fixed coordinates relative to one another. Purine and pyrimidine bases in polynucleotides or peptide planes in polypeptides are rigid bodies in the above sense. Consider a biopolymer containing two rigid bodies that are at close proximity. Assume that located within each rigid body is a spin-1/2 nucleus with an associated CSA tensor. If each CSA tensor can be oriented relative to a frame fixed to each rigid body by a DQDRAWS experiment, which detects the mutual orientation of the two CSA tensors through the evolution of the double quantum coherent state, the mutual orientation of the two rigid bodies is also determined. This strategy will be used, in the following sections to determine the mutual orientation of pyrimidine bases in a DNA oligomer.

III. EXPERIMENTAL METHODS

A. NMR spectroscopy

All MAS experiments were performed on a home-built NMR spectrometer operating at a ^{13}C NMR frequency of 100.53 MHz. A 5 mm Doty Scientific MAS probe was used for room temperature experiments and a Chemagnetics 5 mm MAS probe was used for low temperature experiments. Sample spinning rate was stabilized to within ± 2 Hz with a home-built spin rate controller. During cross polarization, the ^{13}C rf level was set to 60–62.5 kHz, and the proton power level was set to achieve a Hartmann–Hahn match.³⁹ During the application of the DRAWS sequence the ^{13}C rf power was decreased to 38.5 kHz, and during the t_1 and t_2 periods the proton decoupling level was set to 100–120 kHz. ^{13}C pulses were delivered by a Kalmus LP1000 amplifier. Proton pulses were delivered by a Henry Radio 2004-A amplifier. A standard tune-up sequence was used to minimize pulse errors.⁴⁰ Phase cycling was used to eliminate signal which did not pass through a double quantum state during the evolution period. Two dimensional spectra were acquired in hypercomplex mode⁴¹ and the DQDRAWS spectrum was obtained by selective projection of ω_2 columns.

Powder patterns were acquired on a home-built NMR spectrometer operating at a ^{13}C Larmor frequency of 50.3 MHz. Cross polarization fields were set to 62 kHz for both ^{13}C and ^1H channels. The proton decoupling field was set to

125 kHz and the ^{15}N decoupling field was set to 20 kHz. A MREV-8⁴² sequence was used for the dipolar modulation experiment. During the MREV-8 sequence, the proton 90° pulse time was $1.6\ \mu\text{s}$ and a complete MREV-8 cycle was $24.7\ \mu\text{s}$ long.

In all rotational resonance experiments the initial state $I_z - S_z$ was prepared by selective inversion accomplished with the four 180° -pulse sequence of Geen, Levitt, and Bodenhausen⁴³ and a 90° pulse. A second 90° read out pulse terminated the mixing period. A 16-step phase cycle was used to eliminate signal which did not go through a zero quantum state during the mixing period. Chemical shift scaling⁴⁴ was used during acquisition to eliminate spectral overlap.

B. Sample preparation

Methods used to make: 2'-deoxythymidine- $2\text{-}^{13}\text{C}\text{-}1,3\text{-}^{15}\text{N}_2$, 2'-deoxythymidine- $4\text{-}^{13}\text{C}\text{-}1,3\text{-}^{15}\text{N}_2$, 2'-deoxythymidine- $6\text{-}^{13}\text{C}\text{-}1,3\text{-}^{15}\text{N}_2$, 2'-deoxythymidine- $4,6\text{-}^{13}\text{C}_2\text{-}1,3\text{-}^{15}\text{N}_2$, and 2'-deoxythymidine- $2,4\text{-}^{13}\text{C}_2\text{-}1,3\text{-}^{15}\text{N}_2$ were adapted from the procedures of Redwine and Whaley⁴⁵ and Williamson and Boxer.⁴⁶ Condensation of the silylated base with the 3',5'-ditoluy chlorodeoxyribose followed by crystallization and deprotection results in the β -anomer of 2'-deoxythymidine.⁴⁷

^{13}C and ^{15}N -labeled β -cyanoethylphosphoramidites were prepared using methods described previously.⁴⁸ Singly labeled thymidine phosphoramidites were incorporated into nucleotide positions T7 and T8 in the DNA dodecamer $[d(\text{CGCGAAT}^*\text{T}^*\text{CGCG})]_2$ with an Applied Biosystems 392 DNA synthesizer in two $10\ \mu\text{mol}$ batches, and were purified by methods described in a previous publication.⁴⁹ DNA samples were dissolved in a buffered, aqueous solution, and for solid-state NMR studies were cooled to $-120\ ^\circ\text{C}$ in an Chemagnetics CPMAS probe using liquid nitrogen boil-off.

IV. RESULTS

A two-step strategy was used to determine the mutual orientation of pyrimidine bases in DNA from DQDRAWS. First, the $^{13}\text{C}_2$, $^{13}\text{C}_4$, and $^{13}\text{C}_6$ CSA tensors in 2'-deoxythymidine were oriented in a frame fixed to the pyrimidine ring. Then, from the DQDRAWS spectrum of a coupled ^{13}C spin pair in DNA, the mutual orientation of the CSA tensors of ^{13}C spins on separate pyrimidine bases and thus the mutual orientation of the pyrimidine bases was determined.

Single crystals of 2'-deoxythymidine could not be prepared in sufficient size for NMR study. Therefore, the orientation of the CSA tensors for the $^{13}\text{C}\text{-}2$, $^{13}\text{C}\text{-}4$, and $^{13}\text{C}\text{-}6$ in polycrystalline 2'-deoxythymidine were obtained using a combination of static powder pattern analysis, separated local field spectroscopy and DQDRAWS. The results of the DQDRAWS analysis were checked using a combination of static powder pattern analysis, first- and second-order rotational resonance.

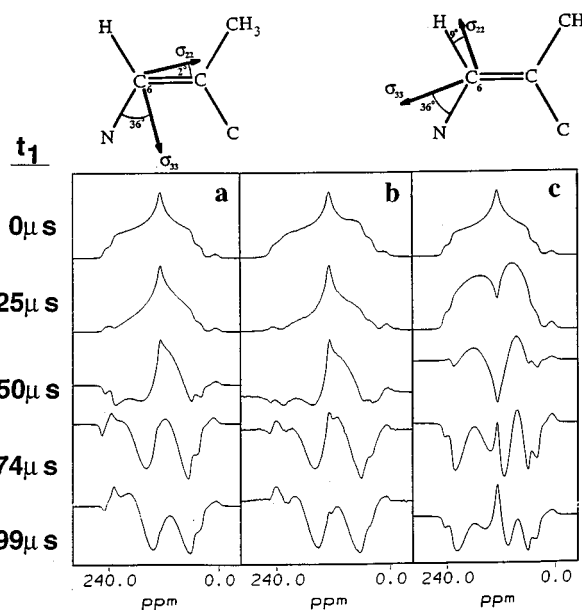


FIG. 4. Dipolar modulation experiment performed on 2'-deoxythymidine- $6\text{-}^{13}\text{C}$. Duration of the MREV-8 irradiation is t_1 . (a) The best fit calculated spectrum and the corresponding C6 CSA tensor orientation; (b) Experimental dipolar modulation data; (c) An alternative model for the C6 CSA tensor orientation.

A. Determination of ^{13}C chemical shielding tensor orientations in 2'-deoxythymidine by powder pattern analysis, dipolar modulation, and rotational resonance

To determine the orientation of the ^{13}C CSA tensors of C2, C4, and C6 with respect to the local molecular frame fixed to the thymine ring, it is convenient to begin with a ^{13}C spin that is directly-bonded to two heterospins. The CSA tensor of that spin is then oriented relative to the two bond axes. Because the C-6 carbon in thymidine is protonated and is directly bonded to $^{15}\text{N}1$, it was possible to perform a dipolar modulation experiment to orient the C6-H and C6-N1 bonds in the PAS of C-6's CSA tensor.⁵⁰ For the olefinic $^{13}\text{C}\text{-}6$ carbon it is assumed that the most shielded tensor element σ_{11} is perpendicular to the plane of the ring.⁵¹ This assumption and the ^{15}N coupled data indicate that the σ_{33} element of C6's CSA tensor makes an angle of 36° to the C6-N1 bond with σ_{22} almost parallel to the C5-C6 bond. Figure 4 shows the data on the right and the best fit simulation on the left.

A rotational resonance experiment was then used to determine the orientation of $^{13}\text{C}\text{-}4$'s CSA tensor relative to C-6's CSA tensor. Rotational resonance is insensitive to CSA tensor orientations if the chemical shift anisotropies of the labeled spins are small compared to the rotor speed.⁵² However, this is not the case for 2'-deoxythymidine- $4,6\text{-}^{13}\text{C}_2$ even at first-order rotational resonance, $\Delta\sigma_{\text{ISO}} = \nu_R$ because for $^{13}\text{C}_4$ and $^{13}\text{C}_6$ the isotropic chemical shift difference $\Delta\sigma_{\text{ISO}} = 29\ \text{ppm}$ and the anisotropies for both CSA tensors exceed $75\ \text{ppm}$. We were able to use this fact to our advantage since the distance, and hence the dipolar coupling strength between the two ^{13}C labels, is known from x-ray

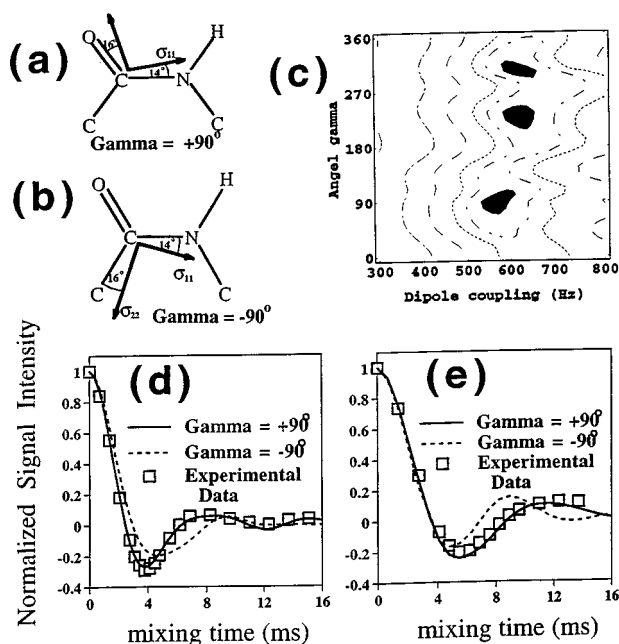


FIG. 5. Results of rotational resonance experiments performed on 2'-deoxythymidine-4,6- $^{13}\text{C}_2$. (a) ^{13}C -4 chemical shift tensor orientation for $\gamma = +90^\circ$. (b) ^{13}C -4 chemical shift tensor orientation for $\gamma = -90^\circ$. (c) Contour plot showing χ^2 values determined by comparing the results of a first-order rotational resonance experiment and calculated results. The angle γ and the dipolar coupling strength were varied in the calculations. The gray areas indicate the best fit areas where $\chi^2 < 0.04$. Other contour lines represent χ^2 values of 0.08, 0.2, 0.3, 0.4, and 0.5, respectively. (d) Results of the first-order rotational resonance experiment. Squares indicate experimental data. The rotor speed was $\nu_R = 2915$ Hz. The solid and dashed lines are simulated exchange curves for the $\gamma = +90^\circ$ and $\gamma = -90^\circ$ tensor orientations, respectively. (e) Results of a second-order rotational resonance experiment. The rotor speed was $\nu_R = 1458$ Hz.

data. Because C-4 is a carbonyl carbon and is a member of a heterocyclic ring, its most shielded CSA tensor element σ_{33} is assumed to be approximately perpendicular to the plane of the thymine ring.⁵¹ The only unknown quantity was the angle γ which rotates the CSA tensor of C4 about the C4-N3 bond.

From the ^{13}C - ^{15}N coupled powder pattern experiment the angle between the σ_{11} element of C4's CSA tensor and the C4-N3 bond was found to be 14° (data not shown). Assuming σ_{33} is orthogonal to the plane of the thymine ring, two possible orientations of C4's CSA tensor exist, corresponding to two values of the angle γ . Figures 5(a) and 5(b) show the orientation of the ^{13}C -4 CSA tensor for $\gamma = 90^\circ$ and $\gamma = -90^\circ$, respectively. To determine the correct value of γ , rotational resonance data were acquired. Figure 5(c) shows a χ^2 surface for a first-order rotational resonance experiment performed on thymidine-4,6- $^{13}\text{C}_2$. To calculate χ^2 , data was compared to calculated exchange curves in which the angle γ and the dipolar coupling constant have been varied. The gray areas indicate the best fit between calculated data and experiment. Since the dipolar coupling constant is known to be 557 Hz, γ must be approximately equal to 90° . Figures 5(d) and 5(e) show first- and second-order rotational resonance ex-

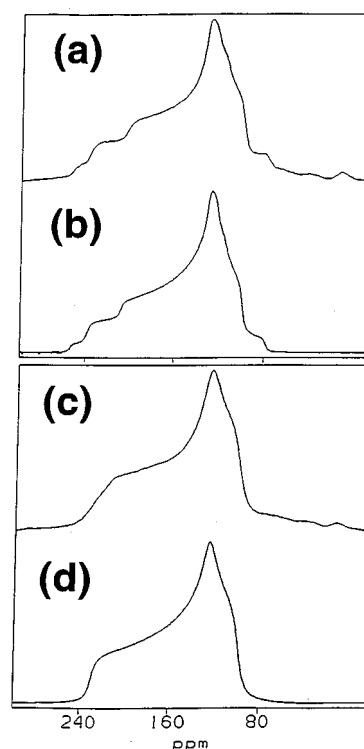


FIG. 6. Static spectra of 2'-deoxythymidine-2- ^{13}C -1,3- $^{15}\text{N}_2$. (a) ^{15}N -coupled spectrum. (b) Best fit calculated ^{15}N -coupled spectrum. (c) ^{15}N -decoupled spectrum. (d) Best fit calculated ^{15}N -decoupled spectrum.

change curves for thymidine-4,6- $^{13}\text{C}_2$. Calculated curves for $\gamma = \pm 90^\circ$ are shown for comparison.

The ^{13}C label in the thymidine-2- ^{13}C sample is adjacent to two ^{15}N labels. This fact allowed the ^{13}C -2 CSA tensor orientation to be completely determined from the ^{15}N coupled spectrum. Figure 6 shows ^{15}N coupled and uncoupled spectra with simulations. The orientation determined from these spectra was in agreement with the results of a rotational resonance experiment performed on thymidine-2,4- $^{13}\text{C}_2$ (data not shown). The orientations for all three ^{13}C tensors are shown in Fig. 7.

B. Determination of ^{13}C chemical shielding tensor orientation in 2'-deoxythymidine by DQDRAWS spectroscopy

The determination of CSA tensor orientation in 2'-deoxythymidine using DQDRAWS is straightforward and begins in the same way as the process described in Sec. IV A. The orientation of C6's CSA tensor is determined relative to a frame fixed to the thymine ring by a dipolar modulation experiment. Then the relative orientation of the CSA tensors of C4 and C2 are determined from DQDRAWS data, first using a DQDRAWS experiment applied to 2'-deoxythymidine-4,6- $^{13}\text{C}_2$ to determine the orientation of C4's CSA tensor to C6's CSA tensor, then applying DQDRAWS to 2'-deoxythymidine-2,4- $^{13}\text{C}_2$ to determine the mutual orientation of the C2 and C4 CSA tensors.

In Fig. 8 experimental DQDRAWS spectra for 2'-deoxythymidine-2,4- $^{13}\text{C}_2$ and 2'-deoxythymidine-

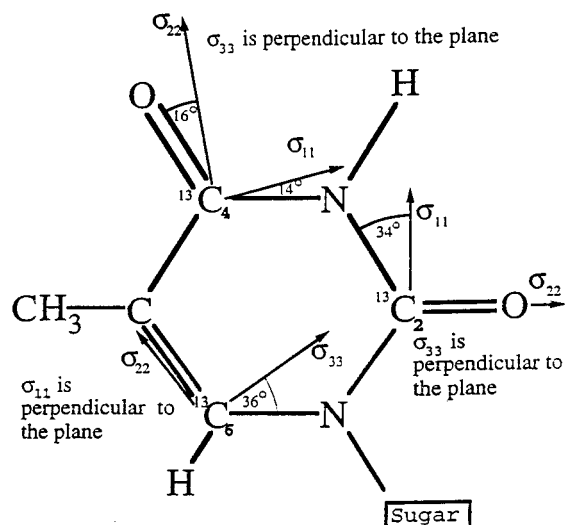


FIG. 7. Diagram showing the chemical shift tensor orientations for the ^{13}C -2, ^{13}C -4, and ^{13}C -6 carbons in 2'-deoxythymidine. Angles are accurate to within five degrees. The principal tensor values are, for ^{13}C -2, $\sigma_{11} = 227$ ppm, $\sigma_{22} = 122$ ppm, $\sigma_{33} = 96$ ppm; for ^{13}C -4, $\sigma_{11} = 242$ ppm, $\sigma_{22} = 168$ ppm, $\sigma_{33} = 89$ ppm; and for ^{13}C -6, $\sigma_{11} = 49$ ppm, $\sigma_{22} = 130$ ppm, $\sigma_{33} = 238$ ppm. The convention $|\sigma_{33} - \sigma_{\text{ISO}}| > |\sigma_{11} - \sigma_{\text{ISO}}| > |\sigma_{22} - \sigma_{\text{ISO}}|$ has been followed. Tensor values are referenced to TMS and are accurate to within two ppm.

$4,6$ - $^{13}\text{C}_2$ are shown along with calculated double quantum spectra. Double quantum spectra were calculated using the tensor orientations displayed in Fig. 7. Agreement between theory and experiment is excellent.

To further check the consistency of the tensor orientations, the orientation of the CSA tensor of $^{13}\text{C}2$, determined from the data in Fig. 6, was assumed as a starting point and the orientation of the $^{13}\text{C}4$ CSA tensor relative to the molecular frame was derived from the DQDRAWS spectrum of 2'-deoxythymidine-2,4- $^{13}\text{C}_2$ shown in Fig. 8. Now the orientation of the CSA tensor of $^{13}\text{C}6$ was determined by calculating the DQDRAWS spectrum for 2'-deoxythymidine-4,6- $^{13}\text{C}_2$ as a function of ξ , the angle between the σ_{33} axis of C-6's CSA tensor and the C6-N1 bond [Fig. 9(a)]. To quantify the goodness of fit between simulation and experiment a residual function χ^2 was defined as the sum of the square of the differences between all pairwise ratios of intensities for the experimental (I_i^{expt}) and simulated (I_i^{sim}) spectra

$$\chi^2 = \frac{1}{2(2m+1)} \sum_{i=-m}^{+m} \sum_{j>i} \frac{(I_j^{\text{expt}}/I_i^{\text{expt}} - I_j^{\text{sim}}/I_i^{\text{sim}})^2}{I_j^{\text{sim}}/I_i^{\text{sim}}}. \quad (20)$$

Figure 9(b) is the plot of χ^2 as a function of ξ for the DQDRAWS series shown in Fig. 9(a) compared to the DQDRAWS data in Fig. 8. The angle of $\xi = 36^\circ$ is at a minimum in the χ^2 plot, which is consistent with the results of $^1\text{H}6$ - $^{13}\text{C}6$ - $^{15}\text{N}1$ dipolar modulation experiment.

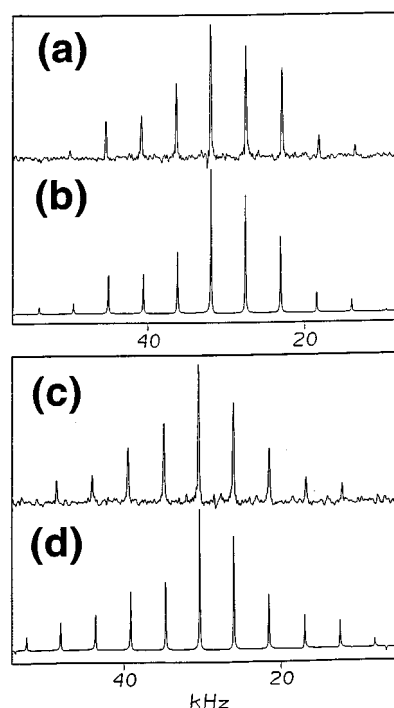


FIG. 8. Double quantum projections. In all projections given in this figure, the preparation time was 1.768 ms and the rotor speed was set to $\nu_R = 4525$ Hz. (a) Experimental double quantum projection of 2'-deoxythymidine-2,4- $^{13}\text{C}_2$. (b) Calculated double quantum projection of 2'-deoxythymidine-2,4- $^{13}\text{C}_2$. (c) Experimental double quantum projection of 2'-deoxythymidine-4,6- $^{13}\text{C}_2$. (d) Calculated double quantum projection of 2'-deoxythymidine-4,6- $^{13}\text{C}_2$.

C. Determination of the mutual orientation of two thymine rings in $[d(\text{CGCGAAT}^*\text{T}^*\text{CGCG})_2]$ by DQDRAWS spectroscopy

The nature of pyrimidine base stacking in a DNA dodecamer was determined from DQDRAWS data in the following manner. Forty milligrams of the DNA oligomer $[d(\text{CGCGAAT}^*\text{T}^*\text{CGCG})_2]$ were synthesized as described in Sec. IV, with 2'-deoxythymidine-6- ^{13}C -1,3- $^{15}\text{N}_2$ incorporated into position T7 and 2'-deoxythymidine-4- ^{13}C -1,3- $^{15}\text{N}_2$ incorporated into position T8. The $^{13}\text{C}6$ - $^{13}\text{C}4$ internuclear distance, and the mutual orientation of the T7 and T8 pyrimidine rings, is dependent upon the hydration state of the DNA.⁵³ Therefore, the labeled DNA dodecamer was hydrated to a level corresponding to greater than 64 molecules of water per nucleotide, which is sufficient to produce a B-form DNA structure. To attenuate dynamic averaging of the dipolar interaction, the hydrated DNA sample was cooled to -120°C .

The $^{13}\text{C}6$ - $^{13}\text{C}4$ internuclear distance was determined using the DRAWS pulse sequence. The TOSS- τ -deTOSS method of Green *et al.* was used to prepare an initial state $I_y - S_y$.⁵⁴ These data were used as a control to correct the $I_y + S_y$ DRAWS data for relaxation effects and coupling to ^{13}C spins at natural abundance. $I_y - S_y$ and $I_y + S_y$ DRAWS decay data for the doubly labeled DNA dodecamer are shown in Fig. 10 and indicate a C6-C4 distance of 4.0

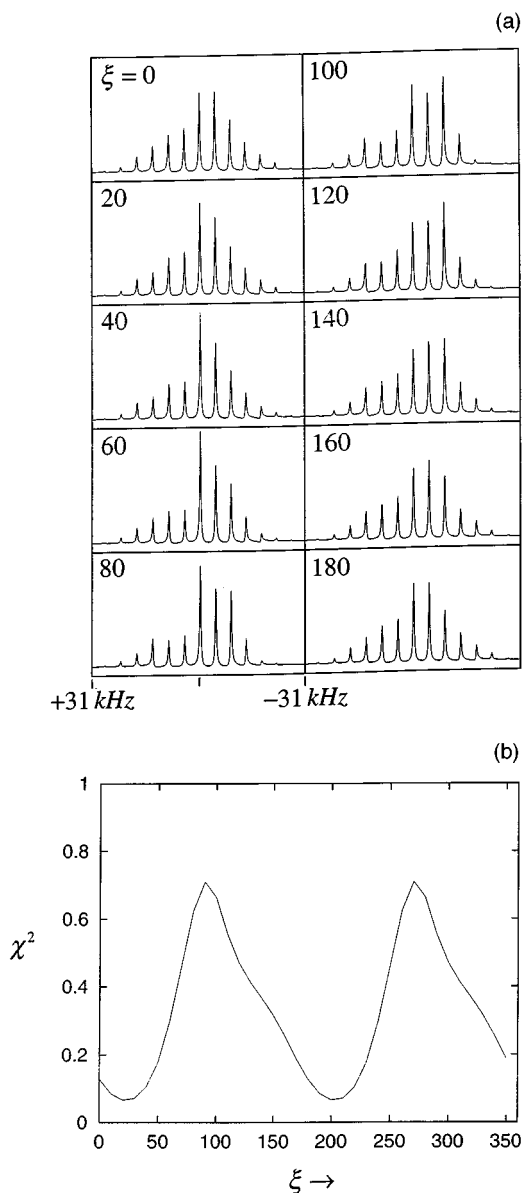


FIG. 9. Sensitivity of the double quantum spectrum of 2'-deoxythymidine-4,6- $^{13}\text{C}_2$ to a change in the mutual orientation of the shift tensors and the uniqueness of the best fit spectrum: (a) double quantum spectrum of 2'-deoxythymidine-4,6- $^{13}\text{C}_2$ as a function of the angle ξ between the σ_{33} axis of the CSA tensor of ^{13}C -6 and the C6-N1 bond; (b) χ^2 plot for best fit spectrum to the experimental data where χ^2 is given by Eq. (20).

± 0.20 Å, in excellent agreement with the distance of 4.20 Å obtained from the solution NMR structure⁵⁵ and the canonical *B*-form distance of 4.26 Å.

The experimental DQDRAWS spectrum of the two coupled ^{13}C spins labels attached to T7 and T8 in $[d(\text{CGCGAAT}^*\text{T}^*\text{CGCG})]_2$ is shown in Fig. 11(b). A simulation of the DQDRAWS spectrum uses: The principal values for the CSA tensors of $^{13}\text{C}6$ and $^{13}\text{C}4$ (Table I), the CSA tensor orientations, and the $^{13}\text{C}6$ - $^{13}\text{C}4$ distance of 4.0 Å, derived from the DRAWS experiment described above. As an initial guess for the orientation of the thymine rings of T7 and T8, it was assumed that the DNA structure in the AATT segment is close to canonical *B* form.⁵⁶ The orien-

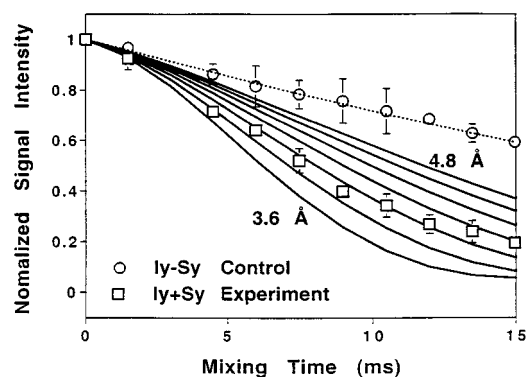


FIG. 10. I_y+S_y and I_y-S_y DRAWS decay curves for $[d(\text{CGCGAAT}^*\text{T}^*\text{CGCG})]_2$, hydrated to a level of 64 water molecules per nucleotide and cooled to -120°C . The DRAWS data best match the 4.0 ± 0.2 Å curve, in excellent agreement with the distance of 4.20 Å, obtained from the high-resolution NMR structure, and the canonical *B*-form distance of 4.26 Å.

tation of each CSA tensor relative to a frame fixed to its thymine ring was derived from the data in Fig. 7. To calculate the Euler angles relating the two CSA tensors, an intermediate frame was defined with the z axis parallel to the C4-C6 internuclear vector. The direction of the x or y axis can be selected arbitrarily and for convenience was oriented such that $\gamma=0^\circ$ for the CSA tensor of the C4 carbon on the T8 nucleotide. Using this convention the Euler angles corresponding to a *B*-form structure are

$$\text{T7:C6 } \alpha=8^\circ, \beta=52^\circ, \gamma=162^\circ$$

and

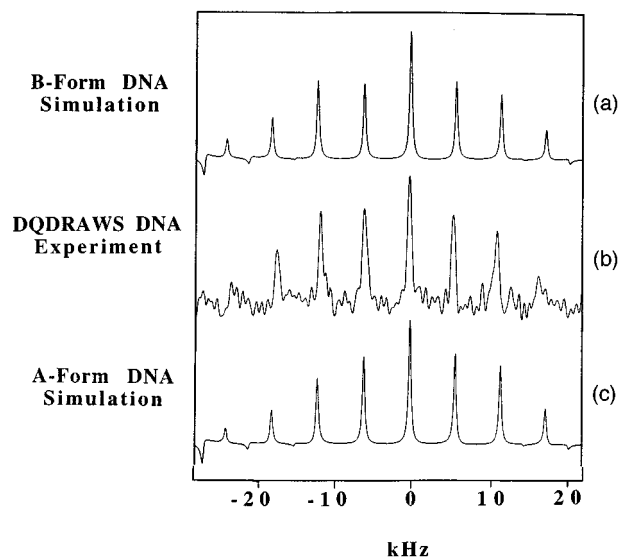


FIG. 11. Calculated and experimental DQDRAWS spectra for $[d(\text{CGCGAAT}^*\text{T}^*\text{CGCG})]_2$, obtained under the same experimental conditions as described in Fig. 10. (a) DQDRAWS simulation assuming an orientation of the T7 and T8 bases found in canonical *B*-form DNA. (b) Experimental DQDRAWS spectrum obtained from the doubly labeled DNA dodecamer; (c) DQDRAWS simulation assuming an orientation of the T7 and T8 bases found in canonical *A*-form DNA. See text for details.

TABLE I. Tensor values for three carbon nuclei in thymidine. The convention $|\sigma_{33} - \sigma_{\text{iso}}| \geq |\sigma_{11} - \sigma_{\text{iso}}| \geq |\sigma_{22} - \sigma_{\text{iso}}|$ has been assumed. The principal tensor values are accurate to ± 2 ppm. θ and ϕ are the polar and azimuthal angles for the $^{13}\text{C}-^{15}\text{N}$ dipole vector. Start with the coupled ^{15}N nucleus placed so the $^{13}\text{C}-^{15}\text{N}$ bond vector is parallel to the σ_{33} axis. First, the angle θ rotates the $^{13}\text{C}-^{15}\text{N}$ vector toward the σ_{11} axis. Then, the angle ϕ rotates the $^{13}\text{C}-^{15}\text{N}$ vector around the σ_{33} axis toward the positive σ_{22} axis. For the C-2 carbon the polar angles relative to N-1 are θ and ϕ the polar angle relative to N-3 are ξ and ζ . Angles are accurate to $\pm 5^\circ$.

Carbon	σ_{11}	σ_{22}	σ_{33}	θ	ϕ	ξ	ζ
^{13}C -2	227 ppm	122 ppm	96 ppm	90°	36°		
^{13}C -4	242 ppm	168 ppm	91 ppm	-14°	90°		
^{13}C -6	44 ppm	130 ppm	238 ppm	-34°	90°	214°	90°

$$\text{T8:C4 } \alpha = 355^\circ, \beta = 37^\circ, \gamma = 0^\circ.$$

The simulated DQDRAWS spectrum is shown in Fig. 11(a). Using Eq. (20) and the five most intense sidebands in Figs. 11(a) and 11(b), it was found that $\chi^2 = 0.017$. For comparison, an A-form structure corresponds to

$$\text{T7:C6 } \alpha = 28^\circ, \beta = 48^\circ, \gamma = 0^\circ$$

and

$$\text{T8:C4 } \alpha = 344^\circ, \beta = 56^\circ, \gamma = 208^\circ.$$

The simulation for the A-form structure is shown in Fig. 11(c) and for this case the fit is poorer, with $\chi^2 = 0.054$.

Although the agreement between the experimental DQDRAWS spectrum and B-form simulation is very good, x-ray⁵⁶ and solution NMR⁵⁵ studies indicate that sequence specific deviations from the canonical B-form structure occur in this DNA sequence. An exhaustive search over all possible orientations and translations of these two bases is beyond the scope of this paper. However, it is possible to demonstrate that the base orientation specified by the canonical B-form structure is indeed at a local minimum in χ^2 space. To explore the form of the DQDRAWS spectrum as a function of local structure, the DQDRAWS spectrum of the doubly labeled DNA dodecamer was simulated as a function of the rotation of T8's base about its glycosidic bond, beginning with canonical B form and incrementing the rotation angle to a maximum of 60° . The position of T7's base is unchanged throughout the rotation series. This simple structural deviation from B form preserves the C4–C6 distance because the position of C4 on T8 is unchanged when T8 is rotated about its glycosidic bond. Although χ^2 increases slightly for small deviations from B form ($< 10^\circ$), χ^2 reaches a minimum value of 0.011 for glycosidic bond rotations of 20° – 30° from B-form before increasing to 0.2181 for a rotation of 60° . A more thorough structural search based on DQDRAWS data will be published elsewhere.

V. DISCUSSION

The experimental results and data analysis in Sec. IV illustrate the degree to which local structure, i.e., base stacking, in DNA can be determined from DQDRAWS data using only two ^{13}C labels per pair of bases. It is interesting to

compare and contrast the DQDRAWS-based strategy for determining structure in a biopolymer, and a nucleic acid in particular, with structural methods based solely upon distance information. To uniquely define the positions of two rigid bodies the coordinates of three atoms in each body must be defined. In principle, the set of distances $\{d_{ij}\}$ between all spins i and j in a system can be converted to coordinates $\{v_i = (x_i, y_i, z_i)\}$ by the analytical expressions

$$v_1 = (0, 0, 0); \quad v_2 = (d_{12}, 0, 0);$$

$$v_3 = \left[\frac{d_{13}^2 - d_{23}^2 + d_{12}^2}{2d_{12}}, (d_{13}^2 - x_3^2)^{1/2}, 0 \right]$$

and for $i = 4 \cdots n$,

$$v_i = \left[\frac{d_{1i}^2 - d_{24}^2 + d_{12}^2}{2d_{12}}, \frac{d_{2i}^2 - d_{3i}^2 - d_{12}^2 + d_{13}^2 + 2x_i(d_{12} - x_3)}{2y_3}, \right. \\ \left. \pm (d_{1i}^2 - x_i^2 - y_i^2)^{1/2} \right]. \quad (21)$$

However, the expressions in Eq. (21) are ill-conditioned in the sense that small changes in the distances can produce large changes in the coordinates,⁵⁷ so in practice, more stable algorithms are used to derive coordinates from distance information.⁵⁸ Nevertheless Eq. (21) can be used to estimate the number of distances required to solve the structural problem described in Sec. IV.

Suppose v_1, v_2 , and v_3 are the coordinates of C2, C4, and C6, respectively, in nucleotide T7, and v_4, v_5 , and v_6 are the coordinates of C2, C4, and C6 in T8. From Eq. (21), 12 distances would be required to define the six atomic coordinates. However, assuming $d_{12}, d_{13}, d_{23}, d_{45}, d_{46}$, and d_{56} are known, the number of distances required to determine the relative locations of the bases of T7 and T8 is reduced to six. Therefore, six ^{13}C labels attached to T7 and T8 and six dipolar recoupling measurements would be required to derive the structural information that the DQDRAWS/DRAWS experiments obtained from just two ^{13}C labels.

Other methods exist that determine structure from dihedral angle information. For example, Brenneman and Cross have described a metric method for determining the structure of polypeptides using dipolar couplings derived by solid state NMR.⁵⁹ The metric method is analogous to the distance geometry method^{57,58} in that the former method exploits the general relationships that angles between vectors must satisfy, while the latter method exploits the general relationships that distances between points must satisfy. In practice, the metric method requires oriented samples of isotopically labeled polypeptides. A manageable number of solutions for the dihedral angles describing the polypeptide secondary structure is obtained by measuring the C_αH , NH, and NC_1 dipolar couplings.

The fact that the metric method of Cross and Brenneman requires oriented samples restricts at present the application of this method to high molecular weight DNA, which can be drawn into fibers.⁶⁰ DNA oligomers can be magnetically oriented,⁶¹ but a cholesteric phase results which is not useful

for the metric approach. We have recently shown that Ramachandran angles may be derived from the DQDRAWS spectra of polypeptides in which adjacent carbonyl C₁ carbons have been labeled with ¹³C.⁶² A similar experiment has been reported by Tycko and co-workers⁶³ who rely on spin diffusion to prepare two spin correlations. Schmidt-Rohr⁶⁴ reported recently the determination of polymer secondary structure using double quantum powder patterns. Clearly, DQDRAWS and the methods described by Tycko *et al.* and Schmidt-Rohr have the potential to extract six times the structural information from a given spin pair (i.e., one distance and five Euler angles) than can be obtained by NMR techniques that only measure internuclear distance.

With regard to the view of the detailed structure of the TT segment of the DNA dodecamer, it is clear that DQDRAWS data can distinguish differences in base orientation that occur between canonical *B*-form DNA where the glycosidic bond angle χ is about -102° , and *A*-form DNA where χ is about equal to -155° . Crystal structures of DNA oligomers in *B*-form indicate however that χ can deviate markedly from -102° . In [*d*(CGCGAATTCGCG)]₂ for example, χ is observed to vary between -90° and -140° , with both T7 and T8 having χ values of about -128° , or just over a -25° deviation from canonical *B*-form.⁶⁵ Although small improvements in χ^2 occur for 20° – 30° rotations of T8's glycosidic bond away from 102° , these small decreases are probably not significant at the signal-to-noise level that is observed in Fig. 11.

It is reasonable to consider what errors might exist that compromise the structural interpretation of the DQDRAWS spectrum. Dipolar couplings to adjacent ¹⁴N and/or ¹⁵N spins may contribute to the double quantum side band intensities in DQDRAWS spectra of ¹³C spins in heterocyclic rings. In the present study all nitrogen sites adjacent to ¹³C spin labels were enriched with ¹⁵N as described above. The dipolar coupling between directly bonded ¹³C and ¹⁵N spins is about 1200 Hz. In general this small dipolar interaction can be easily removed by applying a modest decoupling field to the ¹⁵N spins. We found that in practice even if the ¹⁵N decoupling field was not applied the DQDRAWS data still furnish mutual orientations of tensors in good agreement with control experiments. For example, both the ¹³C6 and ¹³C2 tensors on thymidine were oriented relative to molecule-fixed frames using, as described above, a combination of static powder pattern analysis and local field spectroscopy. The orientation of the ¹³C4 tensor was derived using static powder pattern analysis and rotational resonance, as described above. The orientations of the C2, C4, and C6 tensors derived by these independent methods produced simulated ¹³C4–¹³C6 and ¹³C4–¹³C2 DQDRAWS spectra in excellent agreement with experimental DQDRAWS data.

Another source of concern is that the orientations of the CSA tensors of C4 and C6 relative to a frame fixed to the thymine ring in DNA and in thymidine monomer may differ to some degree. The properties of the C2 and C4 CSA tensors are of particular interest because variations of the orientations and principal values of carbonyl CSA tensors are well documented. For example, in a systematic study of carbonyl

¹³C CSA tensors in a series of five glycy-X dipeptides, the angle between the σ_{11} element and the ¹³C–¹⁵N peptide bond axis was observed to vary from 34.5° to 46.6° ,⁶⁶ or a total range of about 12° . A study by Takegoshi *et al.*⁶⁷ of the effect of intermolecular hydrogen bonding on the CSA tensors of carbonyl ¹³C spins showed that downfield shifts of the σ_{22} element by as much as 50 ppm may occur. This element was in fact observed to vary by almost 20 ppm in the glycy-X series.⁶⁶ However, the σ_{22} element of C4's CSA tensor, the value of which is known to be sensitive to local environment and hydrogen-bonding in particular, is virtually identical in DNA and thymidine monomer (data not shown), and the σ_{11} and σ_{33} elements appear to be virtually identical as well.

VI. CONCLUSIONS

In this paper we have used Floquet theory to describe the recoupling of the dipolar interaction of two spin-1/2 nuclei in an MAS experiment using the DRAWS pulse sequence. In particular, this analytical theory predicts the dipolar scaling of 0.36 and the relative insensitivity of the dipolar recoupling of DRAWS to offset. We have also shown that the combination of DQDRAWS and DRAWS can be used to determine the distance between two ¹³C spins, the three Euler angles relating the two CSA tensors, and the two Euler angles orienting the internuclear vector in the PAS of either CSA tensor. Thus trigonometric functions of the Euler angles which specify the mutual orientation of two rigid bodies in a noncrystalline, unoriented polymer can be determined using only two spin labels.

We have considered in detail the manner in which the DQDRAWS spectrum can be interpreted to yield information on the local structure of unoriented, noncrystalline nucleic acids. In particular, three ¹³C CSA tensors in 2'-deoxythymidine have been characterized and their mutual orientation determined using dipolar modulation and DQDRAWS. The results of this study are in agreement with the orientations determined using dipolar modulation, static powder pattern analysis, and rotational resonance, thus proving the validity of the DRAWS/DQDRAWS method.

At present the Euler angles which determine the mutual orientation of chemical shift tensors can be determined to about $\pm 5^\circ$ from the spectra of small model compounds such as 2'-deoxythymidine. In larger macromolecules angular resolution is somewhat more limited, at least for the spin pairs studied to date in labeled DNA dodecamers. DQDRAWS data can distinguish differences in base stacking between the major structural forms of DNA, but small deviations from *B*-form, such as rotations of the glycosidic bond by less than 30° , cannot at present be determined with confidence in the DQDRAWS data of the ¹³C4 and ¹³C6 spins on adjacent pyrimidine rings in nucleic acid oligomers at magnetic fields of 9.4 T. Independent DRAWS measurements of the C2–C2, C5M–C5M, and C6–C1' distances between T7 and T8 in this same DNA dodecamer suggest the occurrence of deviations from *B*-form in this region.⁶⁸ We therefore anticipate that improvements in the sensitivity of

the 13C4/13C6 DQDRAWS experiments, possibly achieved by repeating DQDRAWS experiments at higher magnetic field, and/or the acquisition of DQDRAWS data from other ¹³C spins on the pyrimidine rings (i.e., ¹³C2) will enable these small sequence-specific effects to be determined with confidence.

In principle, information on the stacking of n singly labeled pyrimidine and/or purine rings can be obtained from $(n-1)$ DQDRAWS/DRAWS experiments. Although the DQDRAWS experiment described in this paper used pairwise labeling, the method can be generalized to a multiply labeled sample. Other possible applications of DQDRAWS include the determination of dihedral angles between ¹³C CSA tensors in furanose rings in nucleic acids, and the determination of Ramachandran angles in polypeptides. This work is in progress.

ACKNOWLEDGMENTS

G.P.D. acknowledges support from NIH Grants PO1GM-32681-11 and RO1GM47802-02. D.M.G. acknowledges support from NIH Training Grant GM08268.

APPENDIX: PERTURBATION THEORY CALCULATION OF THE EIGENVALUES OF THE DRAWS FLOQUET HAMILTONIAN

To derive the DRAWS Floquet Hamiltonian we use the fictitious spin-1/2 operator notation introduced by Vega and co-workers.³⁰ We require a convenient expression for the Fourier expansion of the products. Using the function $\omega_D(t)a_z^{12}(t)$ as an example and using the notation of Weintraub and Vega²⁹ we obtain for instance

$$\omega_D(t)a_z^{13+23}(t) = \sum_{n=-\infty}^{+\infty} z_n^{13+23} e^{-int(\omega_R/4)} \quad (\text{A1})$$

where

$$z_n^{13+23} = \sum_{m=-2}^{+2} \omega_{4m}^D a_{z,n-4m}^{13+23}.$$

Approximate expression for the eigenvalues of the DRAWS Floquet Hamiltonian can be obtained using standard perturbation theory. The Floquet Hamiltonian is assumed to have the form

$$H_F = H_F^{(0)} + \lambda V_F, \quad (\text{A2})$$

where V_F is the perturbation Floquet Hamiltonian. V_F includes all Floquet operators X_n^{pq} , Y_n^{pq} , and Z_n^{pq} for $n \neq 0$ in Eq. (7). $H_F^{(0)}$ includes N^{kk} and all operators of the form Z_0^{pq} in Eq. (7). Then we assume the eigenvalue $\mu_{p,k}$ corresponding to the k th Floquet mode and the p th Zeeman state, and the corresponding eigenvector $|\mu_{p,k}\rangle$ can be expressed as perturbation expansions

$$\mu_{p,k} = \sum_{n=0}^{\infty} \lambda^n \mu_{p,k}^{(n)} \quad \text{and} \quad |\mu_{p,k}\rangle = \sum_{n \neq 0}^{\infty} \lambda^n |\mu_{p,k}^{(n)}\rangle. \quad (\text{A3})$$

Using the expression

$$|\mu_{p,k}^{(n)}\rangle = \hat{R}_{p,k} \left[\hat{V}_F |\mu_{p,k}^{(n)}\rangle - \sum_{s=1}^{nn \neq 0} \mu_{p,k}^{(s)} |\mu_{p,k}^{(n-s)}\rangle \right]$$

to calculate the $(n-1)$ order correction to the eigenfunction, and $\mu_{p,k}^{(n)} = \langle p,k | V_F | \mu_{p,k}^{(n-1)} \rangle$ to obtain the n -order correction to the eigenvalue, where the zeroth-order eigenfunction $|\mu_{p,k}^{(0)}\rangle$ is simply represented as $|p,k\rangle$ and the resolvent operators $R_{i,k}$ have the form³²

$$R_{i,k} = \sum_{j \neq i} \left[\frac{|j,k\rangle \langle j,k|}{\mu_{i,k}^{(0)} - \mu_{j,k}^{(0)}} + \sum_{l \neq k} \left(\frac{|i,l\rangle \langle i,l|}{\mu_{i,k}^{(0)} - \mu_{i,l}^{(0)}} + \frac{|j,l\rangle \langle j,l|}{\mu_{i,k}^{(0)} - \mu_{j,l}^{(0)}} \right) \right], \quad (\text{A4})$$

we obtain the following expression for the second order correction to the eigenvalue corresponding to Zeeman state p and Floquet mode k :

$$\mu_{p,k}^{(2)} = \langle p,k | \hat{V}_F \left\{ \sum_{j \neq i} \left[\frac{|j,k\rangle \langle j,k|}{\mu_{i,k}^{(0)} - \mu_{j,k}^{(0)}} + \sum_{p \neq k} \left(\frac{|i,p\rangle \langle i,p|}{\mu_{i,k}^{(0)} - \mu_{i,p}^{(0)}} + \frac{|j,p\rangle \langle j,p|}{\mu_{i,k}^{(0)} - \mu_{j,p}^{(0)}} \right) \right] \right\} \hat{V}_F |p,k\rangle, \quad (\text{A5})$$

which simplifies to Eq. (7). Using Eq. (7) the following expressions for the eigenvalues $\mu_{i,0} = \mu_{i,0}^{(0)} + \mu_{i,0}^{(2)}$ for the four Zeeman blocks of the Floquet Hamiltonian are obtained:

$$\begin{aligned} \mu_{1,0} &= \mu_{1,0}^{(0)} + \mu_{1,0}^{(2)} \\ &\approx \frac{1}{2} (z_0^{12} + z_0^{13+23}) + \frac{1}{4} \left(\frac{|y_0^{12}|^2}{z_0^{12}} + \frac{2|y_0^{14}|^2}{z_0^{12} + z_0^{13+23}} \right) - \left(\frac{2}{\omega_R} \right)^2 \\ &\quad \times \sum_{k=1}^{\infty} \frac{1}{k^2} [(z_0^{12} + z_0^{13+23})|y_k^{14}|^2 + 2z_0^{12}|y_k^{12}|^2], \end{aligned} \quad (\text{A6a})$$

$$\begin{aligned} \mu_{2,0} &= \mu_{2,0}^{(0)} + \mu_{2,0}^{(2)} \\ &\approx \frac{1}{2} (-z_0^{12} + z_0^{13+23}) \\ &\quad - \frac{1}{4} \left(\frac{|y_0^{12}|^2}{z_0^{12}} + \frac{2|x_0^{23}|^2}{z_0^{12} - 3z_0^{13+23}} + \frac{2|x_0^{24}|^2}{z_0^{12} - z_0^{13+23}} \right) + \left(\frac{2}{\omega_R} \right)^2 \\ &\quad \times \sum_{k=1}^{\infty} \frac{2}{k^2} [z_0^{12}|y_k^{12}|^2 - (3z_0^{13+23} - z_0^{12})|x_k^{23}|^2 \\ &\quad - (z_0^{13+23} - z_0^{12})|x_k^{24}|^2], \end{aligned} \quad (\text{A6b})$$

$$\begin{aligned} \mu_{3,0} &= \mu_{3,0}^{(0)} + \mu_{3,0}^{(2)} \\ &\approx -z_0^{13+23} + \frac{1}{4} \left(\frac{2|x_0^{23}|^2}{z_0^{12} - 3z_0^{13+23}} - \frac{|x_0^{34}|^2}{z_0^{13+23}} \right) - \left(\frac{2}{\omega_R} \right)^2 \\ &\quad \times \sum_{k=1}^{\infty} \frac{2}{k^2} [(z_0^{12} - 3z_0^{13+23})|x_k^{23}|^2 - z_0^{13+23}|x_k^{34}|^2], \end{aligned} \quad (\text{A6c})$$

$$\mu_{4,0} = \mu_{4,0}^{(0)} + \mu_{4,0}^{(2)} \approx \frac{1}{4} \left(-\frac{2|y_0^{14}|^2}{z_0^{12} + z_0^{13+23}} + \frac{2|x_0^{24}|^2}{z_0^{12} - z_0^{13+23}} + \frac{|x_0^{34}|^2}{z_0^{13+23}} \right) + \left(\frac{2}{\omega_R} \right)^2 \sum_{k=1}^{\infty} \frac{1}{k^2} [|y_k^{14}|^2 (z_0^{12} + z_0^{13+23}) - |x_k^{24}|^2 (z_0^{12} - z_0^{13+23}) - 2|x_k^{34}|^2 z_0^{13+23}]. \quad (\text{A6d})$$

Using the fact that $\mu_{i,k} = \mu_{i,0} + k\omega_R$ we obtain the following expression for the Floquet Hamiltonian:

$$H_F \approx \frac{\omega_R}{4} \sum_{k=1}^4 \hat{N}^{kk} + \hat{Z}_0^{12} \left\{ z_0^{12} + \frac{1}{2} \frac{|y_0^{12}|^2}{z_0^{12}} + \frac{|x_0^{24}|^2}{z_0^{12} - z_0^{13+23}} - \left(\frac{4}{\omega_R} \right)^2 \sum_{k=1}^{\infty} \frac{1}{k^2} \left[z_0^{12} |y_k^{12}|^2 - \frac{(z_0^{12} - z_0^{13+23})}{2} |x_k^{24}|^2 \right] \right\} + \hat{Z}_0^{13} \left\{ z_0^{13+23} + \frac{1}{2} \frac{|x_0^{34}|^2}{z_0^{13+23}} - z_0^{13+23} \left(\frac{4}{\omega_R} \right)^2 \sum_{k=1}^{\infty} \frac{|x_k^{34}|^2}{k^2} \right\} + \hat{Z}_0^{23} \left\{ z_0^{13+23} - \frac{|x_0^{23}|^2}{z_0^{12} - 3z_0^{13+23}} + (z_0^{12} - 3z_0^{13+23}) \left(\frac{4}{\omega_R} \right)^2 \sum_{k=1}^{\infty} \frac{|x_k^{23}|^2}{k^2} \right\} + \hat{Z}_0^{14} \left\{ -\frac{|x_0^{24}|^2}{z_0^{12} - z_0^{13+23}} - \frac{1}{2} \frac{|x_0^{34}|^2}{z_0^{13+23}} + \frac{|y_0^{14}|^2}{z_0^{12} + z_0^{13+23}} + \left(\frac{4}{\omega_R} \right)^2 \sum_{k=1}^{\infty} \frac{1}{k^2} \left[z_0^{13+23} |x_k^{34}|^2 + \left(\frac{z_0^{12} - z_0^{13+23}}{2} \right) |x_k^{24}|^2 + \left(\frac{z_0^{12} + z_0^{13+23}}{2} \right) |y_k^{14}|^2 \right] \right\}. \quad (\text{A7})$$

For the DRAWS pulse sequence the dipolar terms $y_0^{12} = x_0^{23} = 0$. In addition, if the CSA is zero the chemical shift terms $y_0^{14} = x_0^{24} = x_0^{34} = 0$. Thus we obtain a simplified form for the DRAWS Floquet Hamiltonian

$$H_F \approx \frac{\omega_R}{4} \sum_{k=1}^4 N^{kk} + Z_0^{12} \left\{ z_0^{12} - \left(\frac{4}{\omega_R} \right)^2 \sum_{k=1}^{\infty} \frac{1}{k^2} \left[z_0^{12} |y_k^{12}|^2 - \frac{(z_0^{12} - z_0^{13+23})}{2} |x_k^{24}|^2 \right] \right\} + Z_0^{13} \left\{ z_0^{13+23} - z_0^{13+23} \left(\frac{4}{\omega_R} \right)^2 \sum_{k=1}^{\infty} \frac{|x_k^{34}|^2}{k^2} \right\} + Z_0^{14} \left\{ \left(\frac{4}{\omega_R} \right)^2 \sum_{k=1}^{\infty} \left[\frac{1}{k^2} \left[z_0^{13+23} |x_k^{34}|^2 + \left(\frac{z_0^{12} - z_0^{13+23}}{2} \right) |x_k^{24}|^2 + \left(\frac{z_0^{12} + z_0^{13+23}}{2} \right) |y_k^{14}|^2 \right] \right\} \right\} \times Z_0^{23} \left\{ z_0^{13+23} + (z_0^{12} - 3z_0^{13+23}) \left(\frac{4}{\omega_R} \right)^2 \sum_{k=1}^{\infty} \frac{|x_k^{23}|^2}{k^2} \right\}. \quad (\text{A8})$$

Finally, using the relationship $\hat{Z}_0^{2-3} = \hat{Z}_0^{2-1} + \hat{Z}_0^{1-3} = -\hat{Z}_0^{1-2} + \hat{Z}_0^{1-3}$ we obtain Eq. (8)

$$H_F \approx \frac{\omega_R}{4} \sum_{k=1}^4 N^{kk} + Z_0^{12} \left\{ z_0^{12} - z_0^{13+23} - \left(\frac{4}{\omega_R} \right)^2 \sum_{k=1}^{\infty} \frac{1}{k^2} \left[z_0^{12} |y_k^{12}|^2 + (z_0^{12} - 3z_0^{13+23}) |x_k^{23}|^2 - \frac{(z_0^{12} - z_0^{13+23})}{2} |x_k^{24}|^2 \right] \right\} + Z_0^{13} \left\{ 2z_0^{13+23} - \left(\frac{4}{\omega_R} \right)^2 \sum_{k=1}^{\infty} \frac{1}{k^2} [z_0^{13+23} |x_k^{34}|^2 - (z_0^{12} - 3z_0^{13+23}) |x_k^{23}|^2] \right\} + Z_0^{14} \left\{ \left(\frac{4}{\omega_R} \right)^2 \sum_{k=1}^{\infty} \left[\frac{1}{k^2} \left[z_0^{13+23} |x_k^{34}|^2 + \left(\frac{z_0^{12} - z_0^{13+23}}{2} \right) |x_k^{24}|^2 + \left(\frac{z_0^{12} + z_0^{13+23}}{2} \right) |y_k^{14}|^2 \right] \right\} \right\}. \quad (\text{A9})$$

¹V. W. Hughes and J. S. Geiger, *Phys. Rev.* **99**, 1842 (1995).

²W. A. Anderson, *Phys. Rev.* **104**, 850 (1956).

³J. I. Kaplan and S. Meiboom, *Phys. Rev.* **106**, 499 (1957).

⁴W. P. Aue, E. Bartholdi, and R. R. Ernst, *J. Chem. Phys.* **64**, 229 (1976).

⁵K. Wuthrich, *NMR of Proteins and Nucleic Acids* (Wiley, New York, 1986).

⁶E. R. Andrew, A. Bradbury, and R. G. Eades, *Nature (London)* **162**, 1659 (1959).

⁷I. J. Lowe, *Phys. Rev. Lett.* **2**, 285 (1959).

⁸M. M. Maricq and J. S. Waugh, *J. Chem. Phys.* **70**, 3300 (1979).

⁹E. R. Andrew, A. Bradbury, R. G. Eades, and V. T. Wynn, *Phys. Lett.* **4**, 99 (1963).

¹⁰M. G. Colombo, B. H. Meier, and R. R. Ernst, *Chem. Phys. Lett.* **146**, 189 (1988).

¹¹A. Kubo and C. A. McDowell, *J. Chem. Soc. Faraday Trans.* **84**, 3713 (1988).

¹²Z.-H. Gan and D. M. Grant, *Mol. Phys.* **76**, 1419 (1989).

¹³D. P. Raleigh, M. H. Levitt, and R. G. Griffin, *Chem. Phys. Lett.* **146**, 71 (1988).

¹⁴A. Kubo, A. Root, and C. A. MacDowell, *J. Chem. Phys.* **93**, 5462 (1990).

¹⁵B. H. Meier and W. L. Earl, *J. Chem. Phys.* **85**, 4905 (1986).

¹⁶U. Piantini, O. W. Sorensen, and R. R. Ernst, *J. Am. Chem. Soc.* **104**, 6800 (1982).

¹⁷N. C. Nielsen, F. Cruzet, R. G. Griffin, and M. H. Levitt, *J. Chem. Phys.* **96**, 5668 (1992).

¹⁸R. Tycko and G. Dabbagh, *J. Am. Chem. Soc.* **113**, 9444 (1991).

¹⁹R. Tycko and S. Smith, *J. Chem. Phys.* **98**, 932 (1993).

²⁰Y. K. Lee, N. D. Kurur, M. Helme, O. G. Johannessen, N. C. Nielsen, and M. H. Levitt, *Chem. Phys. Lett.* **242**, 304 (1995).

²¹D. M. Gregory, G. Wolfe, T. Jarvie, J. Shiels, and G. P. Drobny, *Mol. Phys.* **89**, 1835 (1996).

²²H. Geen, J. J. Titman, J. Gottwald, and H. W. Spiess, *Chem. Phys. Lett.* **227**, 79 (1994).

²³H. Green, J. J. Titman, J. Gottwald, and H. W. Spiess, *J. Magn. Reson. A* **114**, 264 (1995).

- ²⁴D. M. Gregory, D. J. Mitchell, J. A. Stringer, S. Kiihne, J. C. Shiels, J. Callahan, M. A. Mehta, and G. P. Drobny, *Chem. Phys. Lett.* **246**, 654 (1995).
- ²⁵G. Floquet, *Ann. de l'Ecole Norm. Sup.* **12**, 47 (1883).
- ²⁶J. H. Poincare, *Les Methodes Nouvelles de la Mechanique Celeste*, Vols. I, II, III, Paris, 1892, 1893, 1899.
- ²⁷J. H. Shirley, *Phys. Rev. B.* **138**, 979 (1965).
- ²⁸M. M. Maricq, *Phys. Rev. B.* **25**, 6622 (1982).
- ²⁹O. Weintraub and S. Vega, *J. Magn. Reson. A* **105**, 245 (1993).
- ³⁰A. Schmidt and S. Vega, *J. Chem. Phys.* **96**, 2655 (1992).
- ³¹D. Dion and J. O. Hirschfelder, *Advances in Chemical Physics Vol. XXXV* (Wiley, New York, 1976).
- ³²A. Kubo and C. A. McDowell, *J. Chem. Phys.* **92**, 7156 (1990).
- ³³T. Nakai and C. A. McDowell, *J. Chem. Phys.* **96**, 3452 (1992).
- ³⁴M. P. Augustine, K. W. Zilm, and D. B. Zax, *J. Chem. Phys.* **98**, 9432 (1993).
- ³⁵G. Goelman, S. Vega, and D. B. Zax, *Phys. Rev. A* **39**, 5725 (1989).
- ³⁶S. Vega, *J. Chem. Phys.* **68**, 5518 (1978).
- ³⁷A. Wokaun and S. Vega, *J. Chem. Phys.* **67**, 1752 (1977).
- ³⁸J. Gottwald, D. E. Demco, R. Graf, and H. W. Spiess, *Chem. Phys. Lett.* **243**, 314 (1995).
- ³⁹A. Pines, M. G. Gibby, and J. S. Waugh, *J. Chem. Phys.* **59**, 569 (1972).
- ⁴⁰D. P. Burum, M. Linder, and R. R. Ernst, *J. Magn. Reson.* **43**, 463 (1981).
- ⁴¹D. J. States, R. A. Haberkorn, and D. J. Ruben, *J. Magn. Reson.* **48**, 286 (1982).
- ⁴²M. E. Stoll, A. J. Vega, and R. W. Vaughn, *J. Chem. Phys.* **65**, 4093 (1976).
- ⁴³H. Geen, M. H. Levitt, and G. Bodenhausen, *Chem. Phys. Lett.* **200**, 350 (1992).
- ⁴⁴A. P. Aue, D. J. Ruben, and R. G. Griffin, *J. Chem. Phys.* **80**, 1729 (1984).
- ⁴⁵C. M. Redwine and T. W. Whaley, *J. Labelled Comp. Radiopharmaceuticals* **16**, 315 (1979).
- ⁴⁶J. R. Williamson and S. J. Boxer, *Nucleic Acids* **16**, 1529 (1988).
- ⁴⁷C. Bhat, in *Synthetic Procedures in Nucleic Acid Chemistry*, edited by W. W. Zorback and R. S. Tipton (Wiley, New York, 1968), Vol. 1, p. 512.
- ⁴⁸A. Kintanar, W.-C. Huang, D. C. Schindele, D. E. Wemmer, and G. P. Drobny, *Biochemistry* **28**, 282 (1989).
- ⁴⁹T. M. Alam and G. P. Drobny, *Biochemistry* **29**, 3421 (1990).
- ⁵⁰C. J. Hartzell, T. K. Pratum, and G. P. Drobny, *J. Chem. Phys.* **87**, 4324 (1987).
- ⁵¹M. Mehring, *Principles of High Resolution NMR in Solids* (Springer, Berlin, 1983).
- ⁵²D. P. Raleigh, M. H. Levitt, and R. G. Griffin, *Chem. Phys. Lett.* **146**, 71 (1988).
- ⁵³T. M. Duncan, *A Compilation of Chemical Shift Tensors* (Farragut, Chicago, 1990).
- ⁵⁴H. Geen, M. H. Levitt, and G. Bodenhausen, *Chem. Phys. Lett.* **200**, 350 (1992).
- ⁵⁵L. Zhu, Ph.D. Thesis, University of Washington, 1994.
- ⁵⁶R. E. Dickerson and H. R. Drew, *J. Mol. Biol.* **149**, 761 (1981).
- ⁵⁷G. M. Crippen, *J. Comp. Phys.* **24**, 96 (1977).
- ⁵⁸G. M. Crippen and T. F. Havel, *Acta Crystallogr. Sect. A* **34**, 282 (1978).
- ⁵⁹M. T. Brenneeman and T. A. Cross, *J. Chem. Phys.* **92**, 1483 (1990).
- ⁶⁰R. Brandes, R. R. Vold, D. R. Kearns, and A. Rupprecht, *Biopolymers* **27**, 1159 (1988).
- ⁶¹T. M. Alam and G. P. Drobny, *J. Chem. Phys.* **92**, 6840 (1990).
- ⁶²M. A. Mehta, P. Bower, D. Gregory, H. Zebroski, and G. P. Drobny, Direct Determination of Protein Backbone Conformation Using Double Quantum Solid State NMR, 37th Experimental NMR Conference, Asilomar, CA (1996).
- ⁶³D. P. Weliky and R. Tycko, *J. Am. Chem. Soc.* **118**, 8487 (1996).
- ⁶⁴K. Schmidt-Rohr, *Macromolecules* **29**, 3975 (1996).
- ⁶⁵H. R. Drew, R. M. Wing, T. Takano, C. Broka, S. Tanaka, K. Itakura, and R. E. Dickerson, *Proc. Natl. Acad. Sci. USA* **78**, 2179 (1981).
- ⁶⁶T. G. Oas, C. J. Hartzell, T. J. McMahon, G. P. Drobny, and F. W. Dahlquist, *J. Am. Chem. Soc.* **109**, 5956 (1987).
- ⁶⁷K. Takegoshi, A. Naito, and C. A. McDowell, *J. Magn. Reson.* **65**, 34 (1985).
- ⁶⁸M. A. Mehta, D. M. Gregory, S. Kiihne, D. J. Mitchell, M. E. Hatcher, J. C. Shiels, and G. P. Drobny, *Solid State Nucl. Magn. Reson.* **7**, 211 (1996).